

# 3D particle positioning from CCD images using the generalized Lorenz–Mie and Huygens–Fresnel theories

J A Guerrero-Viramontes<sup>1</sup>, D Moreno-Hernández<sup>1</sup>,  
F Mendoza-Santoyo<sup>1</sup> and M Funes-Gallanzi<sup>2</sup>

<sup>1</sup> Centro de Investigaciones en Optica A.C., Loma del Bosque 115, Lomas del Campestre, León, Guanajuato 37150, Mexico

<sup>2</sup> AVNTK S.C., Av. Chapalita 1143, Chapalita, Guadalajara, Jalisco 44510, Mexico

E-mail: [chon@cio.mx](mailto:chon@cio.mx)

Received 13 February 2006, in final form 16 June 2006

Published 20 July 2006

Online at [stacks.iop.org/MST/17/2328](http://stacks.iop.org/MST/17/2328)

## Abstract

3D spherical particle positioning is found by using a defocusing method that consists in measuring the central spot size of an experimental image from a particle and comparing its nearest value with a numerically calculated central spot size matrix array. The numerical calculations were carried out using the generalized Lorenz–Mie and the Huygens–Fresnel diffraction theories. On comparison, the experimental results are in good agreement with the predictions made with the numerical calculations and an error analysis is presented.

**Keywords:** diffraction pattern, spherical particle seeding, particle position estimation, PIV

## 1. Introduction

Three-dimensional (3D) positioning of micro spherical particles in 3D velocimetry applications has become an invaluable tool in diverse scientific disciplines such as microbiology, colloidal science and fluid mechanics. In fluid mechanics, 3D particle positioning techniques have increased in number due to their potential applications in studying important technological problems such as mixing and stirring. As a result, many imaging techniques such as stereoscopic imaging [1], holography [2] and quantitative defocusing methods have been developed for particle positioning determination [3–9].

Several methods based on defocusing have been developed to determine the out-of-plane position of spherical particles embedded in a fluid flow. Some of them rely on intensity measurements from an experimental particle image and compare them to numerical calculations where the particle light scattering is modelled using the classical Lorenz–Mie theory [8]; however, light intensity non-uniformities are present in experimental particle images and make the defocus particle extraction difficult. More advanced theoretical and experimental techniques depend on the ability to handle a

more general problem in which the scatter centre is illuminated by a laser beam and have led to the so-called generalized Lorenz–Mie theory (GLMT). The GLMT was used in [5–7]; however, the procedure to extract defocus position is based on an optimization matching algorithm among the experimental and calculated intensity particle images, which makes the procedure a time-consuming task.

There are other approximations where the physical properties of the particles such as the refraction index are neglected to determine the particles' defocus position [3, 4, 9]. A basic model where the defocused position is defined by averaging the intensity of several particles and on comparison to a mathematical expression the final position of the particles is inferred may be found in [4], but it is used for two-dimensional fluid flows and in microscopic systems. Other methods relate the defocused particle position where a modified three-hole aperture was used in conjunction with a commercially available video lens and a CCD camera [3], but it is limited to large particles due to spatial resolution imposed by the experimental set-up. The size change caused by spherical aberration of the outer diffraction ring of a particle image is used to infer the defocused position of particles in [9] but it is used for microscopic systems.

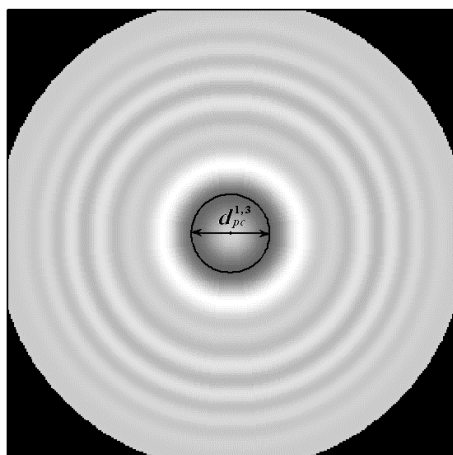


**Figure 1.** Central spot size determination of a calculated particle image diffraction pattern, diameter and defocused position of  $18\ \mu\text{m}$  and  $0.3\ \text{mm}$  respectively.

The approach followed in this investigation is based on the measurement of the central spot size of a particle image. When a spherical particle is imaged it is well known that its diffraction pattern central spot size presents diameter variations due to two parameters: particle size variations and particle defocusing, i.e., away from its focal plane position. Furthermore, it can be shown that central spot changes are more sensitive to particle defocusing position than particle size changes. Consequently, it is possible to use commercially available polydisperse particles (which have a size deviation around a main value) in velocimetry applications and still determine particle position in good agreement only by measuring the central spot size.

The scheme of the proposed method is based on the measurement of the central spot size of a spherical particle image and searching for its nearest value in a matrix array of central spot size calculated numerically using the GLMT and Huygens–Fresnel diffraction theories. This numerical method includes the particle and medium refractive index, shape beam of light illumination and can be used for both micro and macro fluid applications under certain restrictions. The central spot size is typically defined as the first ring in the diffraction pattern of a particle image as in figure 1. The case of a spherical absorbing particle illuminated with monochromatic coherent

light is dealt with. Sets of image data were taken from spherical glass particles, with images ranging from  $0$  to  $+8.0\ \text{mm}$  in  $0.1\ \text{mm}$  steps.

## 2. Experimental arrangement

The experimental set-up devised allows the recording of forward scattering, as in [6], shown in figure 2. The slide used on the particle plane, where the particles are suspended, was antireflection coated to optimize the signal-to-noise ratio (SNR) and was placed on a  $x$ – $y$  translation stage that allowed us to defocus the image. A  $70\ \text{mW}$  He–Ne laser with a  $1.5\ \text{mm}$  waist beam was used with a pair of Newport polarized films to control the laser beam intensity incident on the slide. The lens was a Canon SIGMA 90, which conveyed the particle image onto a plane where a  $640 \times 480$  pixel COHU CCD sensor was placed. Glass sphere particles with diameters ranging from  $20$  to  $30\ \mu\text{m}$ , measured with the Balplan Baush & Lomb microscope, were used to validate the method. This rather large particle size was chosen for convenience of handling only, and if the code was validated for them it can be assumed that it may also be applied and validated for micrometre-sized particles, such as those commonly employed in PIV. The magnification is approximately  $7\times$  in this first step. For practical applications, a low magnification is required in order to achieve adequate interrogation areas. The goal in future work is to use  $4\times$  magnification where the volume that can be imaged will depend on the CCD size sensor and the depth of field needed to be characterized, with  $1\ \text{cm}^3$  expected to be imaged. Several methods were tried to isolate a single particle, a layer of monodisperse polystyrene spheres was deposited on a slide, with a range of sizes tested from  $3\ \mu\text{m}$  to  $13\ \mu\text{m}$ . However, some problems were encountered as the solvent in which the polystyrene spheres were held evaporated, leaving cloudy contours on the slide surface. This noise precluded accurate measurement of diffraction rings. Some were isolated and could be investigated but when defocus was increased nearby particles caused problems. This approach was abandoned.

Glass spherical particles not suspended in a solvent were used. These particles are commercially available in the range from  $10\ \mu\text{m}$  to  $150\ \mu\text{m}$ , and were deposited on a reticule slide and stuck to the glass surface by leaving some residual humidity on the slide. This arrangement worked well for

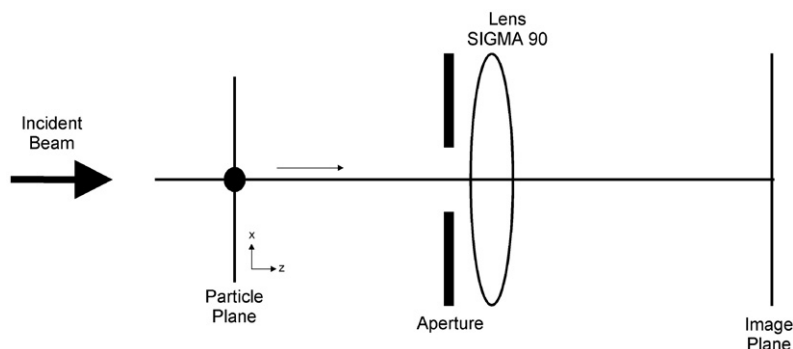


**Figure 2.** Forward scatter set-up for experimental image acquisition.

forward scatter and for large particle sizes. For smaller sizes, less than 10  $\mu\text{m}$ , the system did not yield adequate ring definition due to noise caused by the reticule. So, particles small enough to be of interest and large enough to be easy to handle, in the range of 20  $\mu\text{m}$  to 30  $\mu\text{m}$ , were selected from this distribution.

### 3. Theoretical background

#### 3.1. Particle image calculation

The general approach to the theoretical model can be summarized in three steps. The first step is to calculate the  $x$  component of the external electromagnetic field resulting from the interaction of the incident field with the particle using the exact series expressions presented in an earlier paper by Gouesbet *et al* [10]. Appropriate phase shifts are then introduced, as a second step, to the portions of the external electric fields that are collected by the aperture and imaging lens. After passing through the imaging lens, third step, the electric field can then be propagated onto the image plane through the use of the Fresnel propagation equation.

The GLMT theory has been used to compute the electric field scattered for a spherical, isotropic, homogeneous, nonmagnetic particle [10]. The GLMT describes light scattering by a spherical particle illuminated by a shaped beam. The electric field scattered coming from the particle to the lens aperture is expressed as a function of the following parameters,

$$E = E(\mathbf{x}, \lambda, E_0, d, n, w_0), \quad (1)$$

where  $\mathbf{x}$  is the spatial particle position,  $\lambda$  is the wavelength of the illuminating beam,  $E_0$  is the intensity of the incident electric field upon the particle,  $d$  is the particle diameter,  $n$  is the refractive index and  $w_0$  is the laser beam waist for a shaped beam. Depending on the value of the laser waist,  $w_0$ , the electric field that illuminates the particle can be a plane wave, a Gaussian beam or a light sheet depending on whether  $w_0$  has infinite, finite or two finite values respectively. For the forward scatter set-up configuration used in this research, the total electric field collected by the lens aperture is the sum of the incident electric field on the particle and its scattered electric field.

The propagation of the electric field through the imaging system components is developed from scalar considerations using the thin lens transformation and the Fresnel approximation to the Huygens–Fresnel propagation equation [11]. The equation to calculate the particle image depends on one unknown parameter, namely,

$$E_i = \iint_S E(\lambda, d, E_0, n, w_0) dS, \quad \text{and} \quad I = E_i, E_i^*, \quad (2)$$

where  $E_i$  and  $I$  are the electric field and intensity at the image plane respectively, and the asterisk denotes complex conjugate. To determine  $\mathbf{x}$  for a particle from the intensity of its scattered light, the inverse of equation (2) must be solved. This problem, however, cannot be solved analytically, because equation (2) has no analytical inverse function.

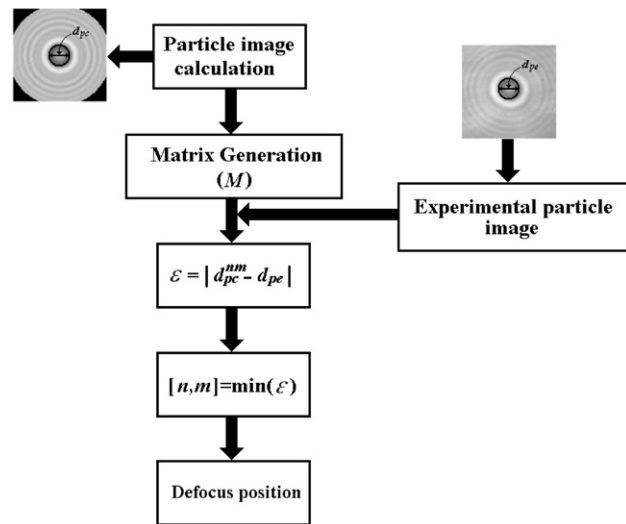


**Figure 3.** A flow chart to determine the defocus position of an experimental particle image.

But it can be solved numerically: the calculation of the electric field,  $E$ , and solution of equation (2) can be found in detail elsewhere [5, 10–13]. Briefly the calculation procedure is as follows. The electric field scattered by the particle and collected by the imaging lens is calculated using the GLMT theory, such that it is exactly known at the entrance of the lens aperture. The electric field is propagated from the lens aperture onwards assuming the paraxial thin lens approximation. Here it is worth recalling that by definition a thin lens is that where a light ray enters and leaves the lens essentially at the same  $x$ - $y$  coordinates. The electric field after the lens is propagated using the Huygens–Fresnel integral. In this research the lens in the imaging system is assumed to be ideal, i.e., free from aberrations.

#### 3.2. The proposed method to determine particle defocus

The scheme for this method is based on the fact that the central spot size of a particle image changes in a regular form by changing the particle diameter or defocusing the particle from its ideal focal plane position. Thus, the particle images for several particle radii and for different defocused positions were computed. The central spot size was measured for each particle radius and defocused position. Then, a matrix array is obtained where columns and rows represent the radius and defocused position for each particle respectively, i.e.,

$$M = \begin{bmatrix} d_{pc}^{11} & \cdot & \cdot & d_{pc}^{1m} \\ \cdot & \cdot & \cdot & \cdot \\ \cdot & \cdot & \cdot & \cdot \\ d_{pc}^{n1} & \cdot & \cdot & d_{pc}^{nm} \end{bmatrix}, \quad (3)$$

where  $M$  is a matrix array,  $d_{pc}^{nm}$  is the central spot size for the particle image calculated,  $n$  and  $m$  are the particle diameter and the defocus position directions, respectively. The central spot size for each particle is determined by selecting the first ring in the diffraction pattern of its image; see figure 1.

The procedure to determine the defocus position of an experimental particle image is depicted in figure 3 as a flow chart. Once the central spot size of an experimental image

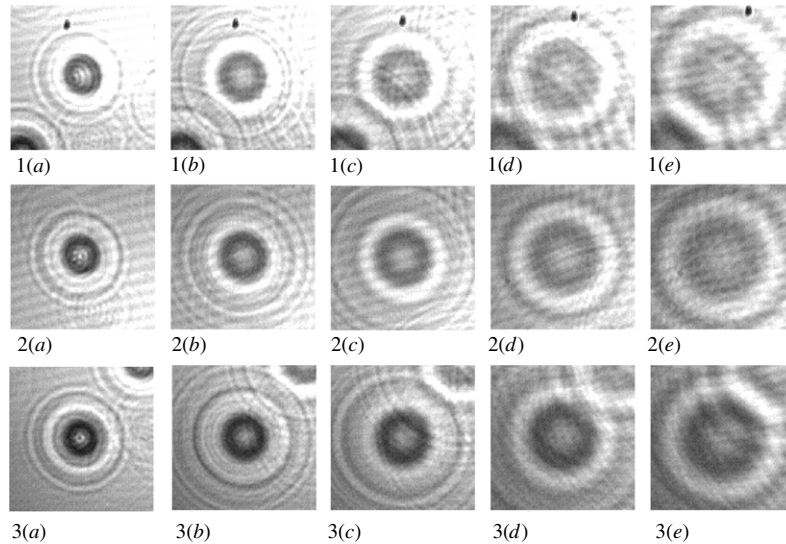


**Figure 4.** Experimental defocused images for three different particle diameters ( $d$ ).  $d_1 = 20.28 \mu\text{m}$  defocused: (1a) 1 mm, (1b) 1.5 mm, (1c) 2 mm, (1d) 3 mm, (1e) 4 mm;  $d_2 = 24.14 \mu\text{m}$  defocused: (2a) 1 mm, (2b) 1.5 mm, (2c) 2 mm, (2d) 3 mm, (2e) 4 mm;  $d_3 = 28.40 \mu\text{m}$  defocused: (3a) 1 mm, (3b) 1.5 mm, (3c) 2 mm, (3d) 3 mm, (3e) 4 mm.

is determined its value is searched in matrix  $M$  using the following condition,

$$\varepsilon = |d_{\text{pc}}^{nm} - d_{\text{pe}}|, \quad (4)$$

where  $\varepsilon$  is a matrix representing the deviation of the real value of the central spot size, and  $d_{\text{pe}}$  is the central spot size of an experimental particle image. The defocus position required is the minimum value of  $\varepsilon$ . Then, by searching for the minimum value of  $\varepsilon$ , the values of  $n$  and  $m$  are obtained and consequently the defocus position of the experimental particle image.

#### 4. Results and discussion

Commercially available monodisperse particles such as polyamide seeding particles, of a specific size,  $20 \mu\text{m}$  PSP-20, have a particle diameter deviation ranging from  $17$  to  $23 \mu\text{m}$ . This large size deviation complicates the position assessment of the particles. Hence, individual particles should be positioned and analysed with microscopic techniques to avoid error measurements and method characterization. For the present research work, the comparison was done between spherical glass particles of sizes  $20.28 \mu\text{m}$ ,  $24.14 \mu\text{m}$  and  $28.4 \mu\text{m}$ , each one for some defocused positions. Figure 4 shows experimental images, acquired using the set-up shown in figure 2, of these particles for several defocused positions. To defocus the image, the particle image plane was moved from its original position by a few millimetres, as given in figure 4. The procedure to calculate the defocus position of experimental images was realized using the condition given by equation (4).

In the analytical model a Gaussian beam with a waist of  $1.5 \text{ mm}$  was considered for particle illumination. The particles whose radius size is from  $9$  up to  $25 \mu\text{m}$  with a step size of  $1 \mu\text{m}$  were used to generate a matrix array of the central spot size. The analysis was made for each particle defocused from its focal plane position at  $0.0 \text{ mm}$  up to  $+8.0 \text{ mm}$  with a step size of  $0.1 \text{ mm}$ . Figure 5 shows the radial intensity of

the particle images when defocus is present. The diffraction pattern formed shows a regular increase of the central spot size by changing the diameter and defocusing the particle. In figure 6 a 3D plot of the variation of the central spot size for several particle diameters and defocus position given by equation (3) is shown. It should be noted that the variation of the central spot size due to the change of the particle diameter is slower than the change due to the defocusing of the particle. In view of that, instead of using monodisperse particles in applications such as 3D particle velocimetry [7], it is possible to use polydisperse spherical particle diameters under certain limits and accurately determine the particle position by using the scheme proposed here. The plot in figure 6 is used as a matrix array,  $M$ , for the determination of the defocus position of an experimental image by measuring only its central spot size.

Figure 7 shows the experimental and numerical comparison for different particle diameters and different particle positions. The results show a reasonable agreement between the experimental and the calculated central spot size. However, deviations are observed between the experimental and numerical results. The mean square error between the experimental and calculated central spot size is found to be  $10.59\%$  for  $20.28 \mu\text{m}$ ,  $9.37\%$  for  $24.14 \mu\text{m}$  and  $7.32\%$  for  $28.40 \mu\text{m}$  experimental particle images used in the experiment. This may be due to approximations made in the model, namely, the assumption of an aberration-free lens, symmetry about the  $z$  axis and the simplified lens transformation. However, having a quantitatively accurate particle imaging model is a step forward in many fields, particularly in velocimetry applications.

#### 5. Error analysis

The uncertainty in the particle defocus position measurement due to errors in measuring the particle defocus position and particle diameter will be characterized in this section. Since

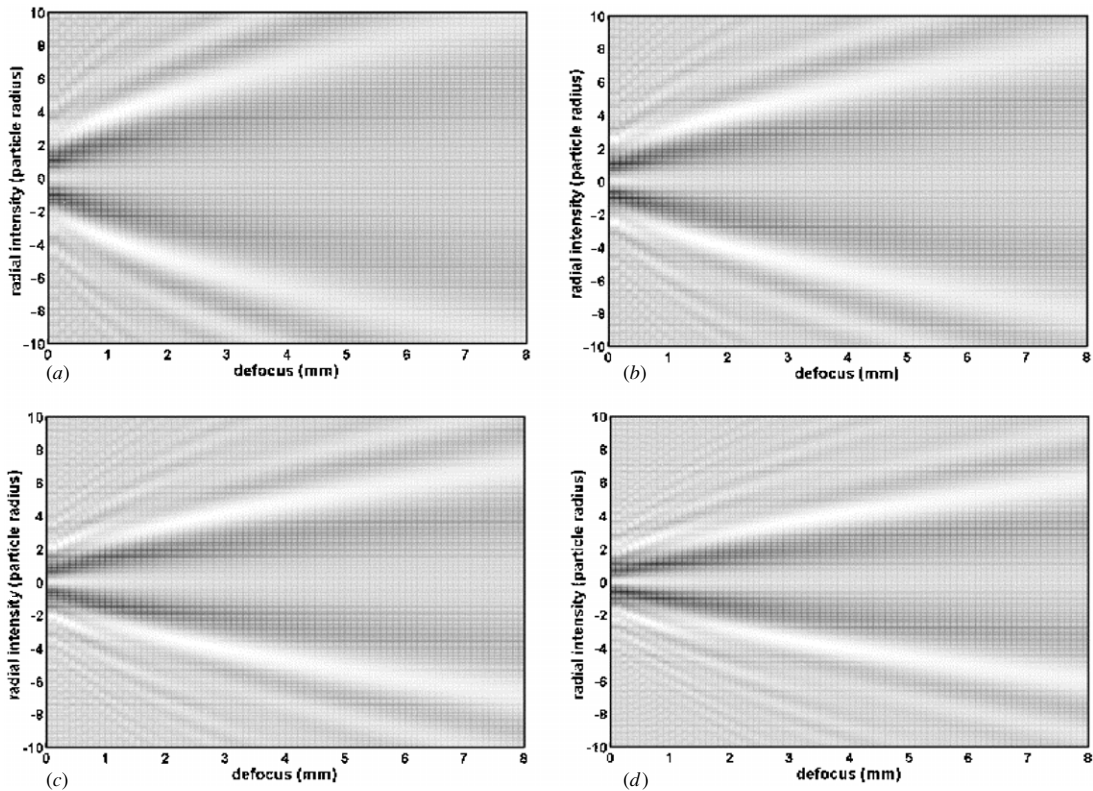


**Figure 5.** Top view of the radial intensity for different defocused spherical glass particles using the GLMT theory model: (a) 20  $\mu\text{m}$ , (b) 24  $\mu\text{m}$ , (c) 28  $\mu\text{m}$  and (d) 32  $\mu\text{m}$  diameter.

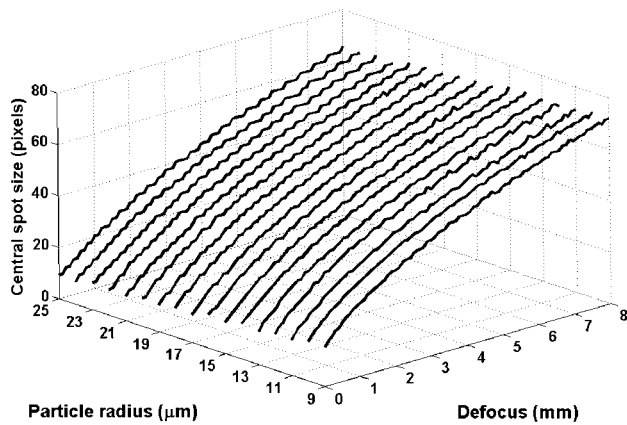


**Figure 6.** 3D plot of the variation of the central spot size when the particle radius increases from 9 to 25  $\mu\text{m}$  in steps of 1  $\mu\text{m}$  and defocus from 0 to 8 mm.

the primary measurement is the central spot size, it is used in the analysis and can be expressed as

$$\alpha = d_{pc}(z_d, d), \tag{5}$$

where  $z_d$  and  $d$  are the defocus position and diameter of a particle, respectively. Let  $\Delta\alpha$  be the error in the particle central spot size measurement, then

$$\Delta\alpha = \frac{\partial d_{pc}}{\partial z_d} \Delta z_d + \frac{\partial d_{pc}}{\partial d} \Delta d, \tag{6}$$

where  $\Delta z_d$  and  $\Delta d$  are the instrument uncertainties. The relative error will therefore be

$$\frac{\Delta\alpha}{\alpha} = \frac{\partial d_{pc}/\partial z_d}{d_{pc}} \Delta z_d + \frac{\partial d_{pc}/\partial d}{d_{pc}} \Delta d. \tag{7}$$

Given that only a single measured value is available, the uncertainty is estimated on the basis of the precision of the instruments from which it was measured. The uncertainty in this case may be smaller than the instrumental precision because it is often possible to interpolate between the smallest subdivisions. Some degree of judgment is required in these instances. A common estimate is one-half to one-tenth of the scale division. In this study one-fifth of the minimum resolution provided by the instruments was used for our analysis. Each instrument used in the experiment has an uncertainty of  $\pm 1.25 \mu\text{m}$  and  $\pm 0.1425 \mu\text{m}$  for the defocus position and particle diameter, respectively.

Equation (7) was used to study errors caused by two parameters, i.e. particle defocus position and particle diameter. The derivatives in equation (7) were evaluated numerically. Tables 1 and 2 show the relative error of each term shown in equation (7): each column corresponds to particle diameter, defocus position and relative error. The columns were ordered such that the largest particle diameter corresponds to the shortest defocus value. This was done to facilitate the observation of the variation of the error by changing particle diameter and defocus position.

The first term of equation (5) shows two effects, the first due to the particle diameter and the second due to the

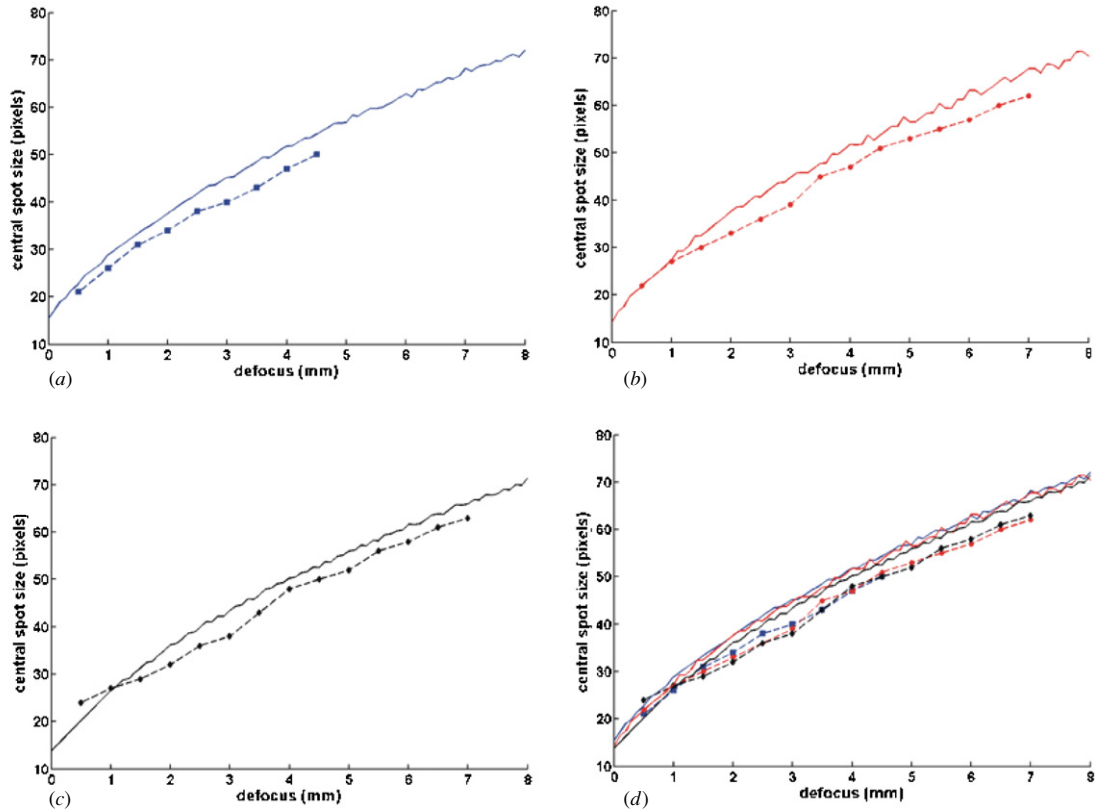


**Figure 7.** Comparison between experimental and calculated central spot size of spherical particle images. The particle diameters are (a)  $20.28\ \mu\text{m}$ , (b)  $24.14\ \mu\text{m}$ , (c)  $28.40\ \mu\text{m}$  and (d) all together.

(This figure is in colour only in the electronic version)

**Table 1.** Relative error for uncertainty measurement in particle defocus position.

$d\ (\mu\text{m})$	$z_d\ (\text{mm})$	Relative error
50	0.0	0.3273
46	1.0	0.2894
42	2.0	0.2518
38	3.0	0.2176
34	4.0	0.1879
30	5.0	0.1623
26	6.0	0.1404
22	7.0	0.1216
18	8.0	0.1054

particle defocus position. Table 1 clearly depicts how the error decreases from the largest to smallest particle diameter and from the shortest to the longest defocus position. These results are consistent with the simulation shown in figures 4 and 5, a larger particle, a small central spot size and consequently more difficulties in determining the central spot size. Also, the error due to the defocusing particle is related to the magnification, thus decreasing the magnification as the error decreases. Table 1 shows a maximum and a minimum error of 32% and 10%, respectively. The second term in equation (5) is related to uncertainty due to the particle diameter. It was mentioned earlier how the slope changes more slowly in the particle diameter direction than in the defocus direction (see figure 6). Therefore the error caused by particle diameter in uncertainty measurement is smaller than the previous one; the value ranges from 0.5% to 0.9% (see

**Table 2.** Relative error for uncertainty measurement in particle diameter.

$d\ (\mu\text{m})$	$z_d\ (\text{mm})$	Relative error
50	0.0	0.0091
46	1.0	0.0088
42	2.0	0.0087
38	3.0	0.0084
34	4.0	0.0079
30	5.0	0.0073
26	6.0	0.0067
22	7.0	0.0061
18	8.0	0.0055

table 2. These results support our previous statement where, instead of using monodisperse particles in applications such as 3D particle velocimetry [7], it is possible to use polydisperse spherical particle diameters under certain limits and determine the particle position with confidence. It is noted that the error in the measurements can be decreased when a small uncertainty in the instruments is available.

## 6. Conclusions

3D particle positioning has been demonstrated using the generalized Lorenz–Mie theory in conjunction with the Huygens–Fresnel propagation theory. The method suggests the possibility of routine accurate 3D velocity estimation by 3D particle positioning determination from 2D camera

images using polydisperse particles instead of monodisperse ones. The code developed and presented here for accurately positioning spherical seeding particles is in good agreement with results found from the experimental set-up.

### Acknowledgments

JAG gratefully acknowledges support from CONACYT and CONCYTEG grants 46975 and 04-K117-038, respectively. DMH gratefully acknowledges support granted by CONACYT and CONCYTEG under contract 47795 and 04-K117-36. FMS would like to acknowledge partial support for this research work through CONACYT grant 42971.

### References

- [1] Racca R G and Dewey J M 1988 A method for automatic particle tracking in a three-dimensional flow field *Exp. Fluids* **6** 25
- [2] Pu Y, Song X and Meng H 2000 Off-axis holographic particle image velocimetry for diagnosing particulate flows *Exp. Fluids* **29** S117–28
- [3] Willert C E and Gharib M 1992 Three-dimensional particle imaging with a single camera *Exp. Fluids* **12** 353–8
- [4] Meinhart C D, Wereley S T and Gray M H B 2000 Volume illumination for two-dimensional particle image velocimetry *Meas. Sci. Technol.* **11** 809–14
- [5] Moreno D, Mendoza-Santoyo F, Guerrero J A and Funes-Gallanzi M 2000 Particle positioning from a single CCD image for application to velocimetry: theory and comparison to experiment *Appl. Opt.* **39** 5117–24
- [6] Guerrero J A, Mendoza-Santoyo F, Moreno D, Funes-Gallanzi M and Fernandez S 2000 Particle positioning from CCD images: experiments and comparison to the generalized Lorenz–Mie theory *Meas. Sci. Technol.* **11** 568–75
- [7] Funes-Gallanzi M 2000 Tunnelling velocimetry: consilience comes to the study of fluid dynamics *10th Int. Symp. on Applications of Laser Techniques to Fluid Mechanics (Instituto Superior Tecnico, Ladoan, 10–13 July)*
- [8] Ovrin B 2000 Three-dimensional forward scattering particle imaging velocimetry applied to a microscopic field-of-view *Exp. Fluids* **29** S175–84
- [9] Wu M, Roberts J H and Buckley M 2005 Three-dimensional fluorescent particle tracking at micron-scale using a single camera *Exp. Fluids* **38** 461–5
- [10] Gouesbet G, Maheu B and Gréhan G 1988 Light scattering from a sphere arbitrarily located in a Gaussian beam, using a Bromwich formulation *J. Opt. Soc. Am. A* **5** 1427–43
- [11] Goodman J W 1968 *Introduction to Fourier Optics* (New York: McGraw-Hill)
- [12] Lock J A 1995 Improved Gaussian beam-scattering algorithm *Appl. Opt.* **34** 559–68
- [13] Schaub S A, Alexander D R and Barton J P 1989 Theoretical model for the image formed by a spherical particle in a coherent imaging system: comparison to experiment *Opt. Eng.* **23** 565–71